Substrate activation for O_2 reactions by oxidized metal centers in biology

Monita Y. M. Pau[†], John D. Lipscomb[‡], and Edward I. Solomon[†§]

[†]Department of Chemistry, Stanford University, Stanford, CA 94305-5080; and [‡]Department of Biochemistry, Molecular Biology and Biophysics and the Center for Metals in Biocatalysis, University of Minnesota, Minneapolis, MN 55455

Edited by Jack Halpern, University of Chicago, Chicago, IL, and approved September 21, 2007 (received for review June 22, 2007)

The uncatalyzed reactions of O_2 (S = 1) with organic substrates (S = 0) are thermodynamically favorable but kinetically slow because they are spin-forbidden and the one-electron reduction potential of O_2 is unfavorable. In nature, many of these important O_2 reactions are catalyzed by metalloenzymes. In the case of mononuclear non-heme iron enzymes, either Fe^{II} or Fe^{III} can play the catalytic role in these spin-forbidden reactions. Whereas the ferrous enzymes activate O_2 directly for reaction, the ferric enzymes activate the substrate for O_2 attack. The enzyme–substrate complex of the ferric intradiol dioxygenases exhibits a low-energy catecholate to Fe^{III} charge transfer transition that provides a mechanism by which both the Fe center and the catecholic substrate are activated for the reaction with O_2. In this Perspective, we evaluate how the coupling between this experimentally observed charge transfer and the change in geometry and ligand field of the oxidized metal center along the reaction coordinate can overcome the spin-forbidden nature of the O_2 reaction.

Mononuclear non-heme iron enzymes perform a wide range of important biological functions involving O_2 in parallel to those of heme enzymes (1–5). Although the uncatalyzed reactions of O_2 (S = 1) with organic substrates (S = 0) are thermodynamically favorable, the reactions are kinetically slow because they are spin-forbidden and the one-electron reduction potential of O_2 is unfavorable. Most of these enzymes catalyze the O_2 reaction by using a high-spin Fe^{II} to activate O_2 through a redox process that also involves the substrate or an additional cofactor providing the required number of electrons. These ferrous O_2-activating enzymes include extradiol dioxygenases, pterin-dependent hydroxylases, α-ketoglutarate-dependent enzymes, and Rieske dioxygenases. However, some mononuclear non-heme iron enzymes possess an oxidized iron active site and use the Fe^{III} to activate substrate for the O_2 reaction. These ferric substrate-activating enzymes presently include the lipoxygenases (LO) and intradiol dioxygenases.

LO employ a relatively straightforward substrate activation mechanism. They catalyze the regio- and stereospecific hydroperoxidation of 1,4-*Z*,*Z*-pentadiene-containing polyunsaturated carboxylic acids (6–10). The resting site of LO consists of a ferrous center coordinated to three histidine ligands, a monodentate C-terminal carboxylate of isoleucine, a carbonyl O of asparagine, and a water (11–13). Resting Fe^{II}LO is oxidized by the hydroperoxide product to Fe^{III}LO, and the water ligand is deprotonated to hydroxide. This Fe^{III}(OH) species catalyzes the first step of the reaction, namely, hydrogen-atom abstraction from the substrate to form a substrate radical, which is accompanied by the reduction of the Fe^{III}(OH) to $Fe^{II}(H_2O)$. The substrate bound near this Fe^{II} site is activated to a radical species (S = 1/2), and its reaction with O_2 (S = 1) is spin-allowed. This step forms a peroxy radical, and then the hydroperoxide product as $Fe^{II}(H_2O)$ is oxidized to Fe^{III}(OH). This mechanism is summarized in Fig. 1 (14, 15). The driving force for the hydrogen-atom abstraction is related to the strength of the OH bond produced in the abstraction intermediate, which is directly related to the reduction potential of the Fe^{III}/Fe^{II} couple ($E°$) and the pK_a of the abstracted proton in the ferrous species. A high reduction potential and a high pK_a of the coordinated water in the reduced species increases the hydrogen-atom abstraction driving force and, hence, the catalytic rate (15–17).

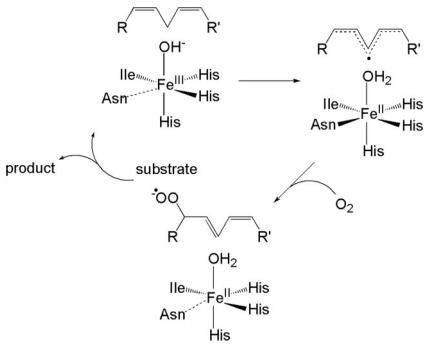

Fig. 1. Mechanism for LO.

The substrate activation mechanism for intradiol dioxygenases is more complex. These enzymes catalyze the cleavage of molecular oxygen accompanied by insertion of both oxygen atoms between the vicinal hydroxyl groups of the catecholic substrate, resulting in ring cleavage to yield muconic acid derivatives (3–5, 18, 19). The resting state of intradiol dioxygenases contains a high-spin ferric center in a distorted trigonal bipyramidal geometry, with Tyr and His as the axial ligands and Tyr, His, and a hydroxide ligand defining the equatorial plane (20–22). Upon anaerobic substrate binding, the active site shifts to a square pyramidal geometry in which the axial Tyr and equatorial OH^- are displaced by the substrate, which binds bidentate in its doubly deprotonated form (23, 24). The open coordination position is trans to the equatorial His, and the substrate binds asymmetric to the Fe^{III} center with the longer bond trans to the equatorial Tyr. EPR and Mössbauer studies have shown that that the iron center remains oxidized and high-spin upon substrate binding (25, 26). Thus direct interaction between the triplet oxygen and the singlet catecholate substrate is still spin-forbidden. Based on different electronic descriptions of the enzyme–substrate (ES) complex, various mechanisms have been proposed for the substrate activation step for the initial O_2 attack in the enzymatic reaction (bracket in Fig. 2): (*i*) Fe^{II}-semiquinone character with O_2 attacking the iron site; (*ii*) Fe^{II}-semiquinone character with O_2 attacking the substrate through radical coupling, and (*iii*) Fe^{III}-catecholate with strong ketonized-character pro-

Author contributions: J.D.L. and E.I.S. designed research; and M.Y.M.P. and E.I.S. performed research, analyzed data, and wrote the paper.

The authors declare no conflict of interest.

This article is a PNAS Direct Submission.

Abbreviations: LO, lipoxygenase; ES, enzyme–substrate; 3,4-PCD, protocatechuate 3,4-dioxygenase; PCA, protocatechuate; 5C, 5-coordinate; 6C, 6-coordinate; SOC, spin-orbit coupling.

[§]To whom correspondence should be addressed. E-mail: edward.solomon@stanford.edu.

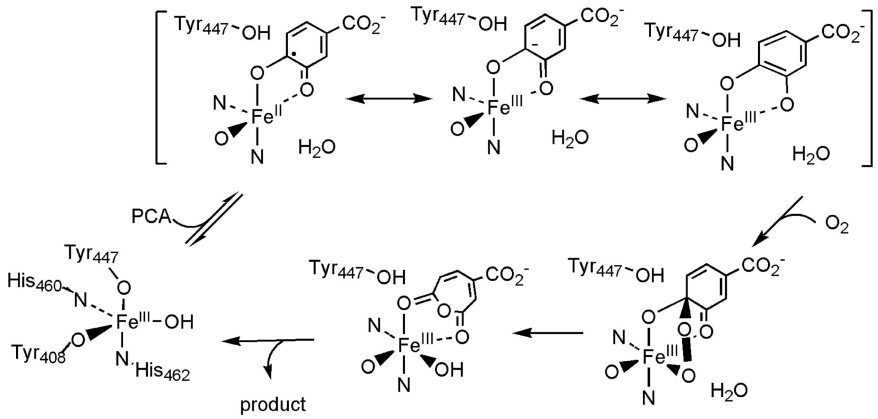

Fig. 2. Intradiol dioxygenases mechanism.

moted by lengthening the Fe–$O^{catechol}$ bond due to the trans effect of the equatorial Tyr, with O_2 directly attacking the substrate through an electrophilic activation (27–33). The net result of the O_2 attack is generally thought to be the formation of a peroxy-adduct bridging between the iron site and one of the hydroxylated carbons of the now quinone that requires a spin-forbidden two-electron transfer of the electron pair of the substrate to the triplet O_2 molecule (23). It is important to determine the mechanism of substrate activation for O_2 reaction in the intradiol dioxygenases both for this class of enzymes and for others where similar mechanisms have been invoked as, for example, in cofactor biogenesis in copper-containing amine oxidases (34, 35).

Because the differences among the substrate activation proposals of intradiol dioxygenases (Fig. 2) lie in the electronic structure description of the ES complex, it was essential to determine the nature of this ES complex experimentally, particularly its degree of radical character. In our previous spectroscopic studies on protocatechuate 3,4-dioxygenase (3,4-PCD) with protocatechuate (PCA) bound, we found that the ES complex is best described as a highly covalent Fe^{III}-catecholate complex with the covalency distributed unevenly among the four valence donor orbitals of the catecholate (36). Because the catecholate has not been fully oxidized to a semiquinone and the oxidation state of the iron remains at the Fe^{III} level (S = 5/2), the reaction with triplet oxygen is still formally spin-forbidden. The combined absorption and magnetic circular dichroism spectra of the ES complex shown in Fig. 3 reflect a very low energy β electron charge transfer transition (the high-spin Fe^{III} has five d electrons with α spin) from the PCA substrate to the Fe^{III} center involving the $\pi_{op\text{-}sym}$ (out-of-plane, symmetric) highest occupied molecular orbital, which is the frontier orbital of the catecholate. This low-energy catecholate to Fe^{III} charge transfer (arrow in Fig. 3) provides a mechanism in which both the Fe center and the catecholic substrate are activated for the reaction with O_2 (36).

In this Perspective, we will consider how this β charge transfer between PCA and the Fe^{III} center and the ligand field of the oxidized metal site in intradiol dioxygenases can overcome the spin-forbidden nature of the two-electron transfer of an electron pair from the highest occupied molecular orbit of the substrate to the triplet O_2 molecule. A reaction coordinate leading to the final intradiol-cleaved product also will be considered.

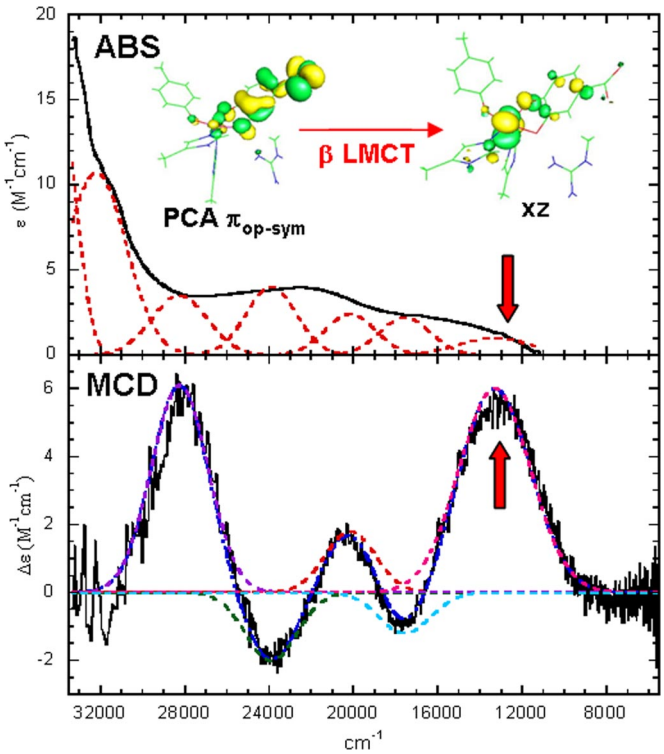

Fig. 3. Absorption (ABS) and magnetic circular dichroism (MCD) spectra of the ES complex of 3,4-PCD.

Nature of the ESO_2 Complex

A two-electron transfer between PCA and O_2 accompanies the formation of the peroxy intermediate bridging between the Fe center and one of the hydroxyl carbons on the catecholic substrate. Direct interaction between the triplet O_2 (S = 1) and the singlet catecholic substrate (S = 0) is formally spin-forbidden. However, EPR studies showed that the ES complex contains a high-spin Fe^{III} center with S_{tot} = 5/2 (25, 26). Hence, the accessible spin states for the O_2 (S = 1) reaction with the ES complex are 3/2, 5/2, and 7/2.

To obtain S_{tot} = 7/2, the O_2 molecule has to be in its $^3\Sigma_g^-$ ground state and ferromagnetically coupled to the high-spin Fe^{III} center for the initial O_2 attack (Fig. 4*A*). This would allow the transfer of a β electron from the occupied PCA $\pi_{op\text{-}sym}$ orbital to the O_2 π^* orbital either directly or through the Fe center. However, the remaining half-occupied PCA $\pi_{op\text{-}sym}$ orbital has an α spin. Transfer of this α electron to the remaining half-occupied O_2 π^* orbital to complete the two-electron redox process is therefore restricted. Geometry optimization of ESO_2 with S_{tot} = 7/2 shows very weak O_2 interactions with both the Fe center and the substrate (Fe–O_2 = 2.42 Å, Fe–C3 = 2.78 Å, Fe–C4 = 2.80 Å). These limited bonding interactions

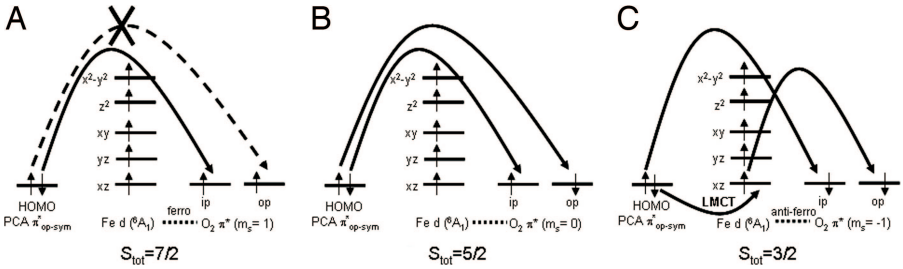

Fig. 4. Schematics of electron transfer in the initial O_2 reaction of intradiol dioxygenases at various spin states: S_{tot} = 7/2 (*A*), S_{tot} = 5/2 (*B*), S_{tot} = 3/2 (*C*).

with the ES complex suggests that the S_{tot} = 7/2 surface is not a favorable path for the initial O_2 reaction.

For S_{tot} = 5/2, the O_2 molecule has to be partially in an excited singlet state (mixed $^1\Delta_g$ and $^1\Sigma_g^+$) at the start of the O_2 reaction (Fig. 4*B*). Because the $^1\Delta_g$ and $^1\Sigma_g^+$ states are ≈1 eV and 1.6 eV higher in energy than the $^3\Sigma_g^-$ ground state of O_2, the initial O_2 reaction with S_{tot} = 5/2 is energetically highly unfavorable.

To obtain S_{tot} = 3/2, the O_2 molecule is in its $^3\Sigma_g^-$ ground state and antiferromagnetically coupled to the high-spin Fe^{III} center for the initial O_2 attack (Fig. 4*C*, d^5 Fe has five α spins and triplet O_2 has two β spins). Spectroscopic data on the ES complex of 3,4-PCD (Fig. 3) (36) showed that the doubly occupied $\pi_{op\text{-}sym}$ orbital of the catecholic substrate PCA is the highest occupied molecular orbital. The high-lying $\pi_{op\text{-}sym}$ orbital of the substrate can readily donate into the O_2 π^* orbital for an electrophilic attack by O_2. However, because O_2 is in its $^3\Sigma_g^-$ state, only the α electron from the doubly occupied $\pi_{op\text{-}sym}$ orbital can be donated directly to the O_2 π^* orbital in the formation of a C^{PCA}–O bond. The second electron required to reduce O_2 to O_2^{2-} has to be donated either by the substrate $\pi_{op\text{-}sym}$ orbital, which would require a forbidden spin-flip of the β electron or by an occupied d orbital (d_{xz}) of the Fe^{III} center, which has α spin and can interact with the remaining half-occupied π^* orbital of O_2 due to their antiferromagnetic coupling. The strong covalent interaction between the PCA $\pi_{op\text{-}sym}$ and d_{xz} orbitals in the β manifold, reflected by the low-energy ligand-to-metal charge transfer transition observed in the spectroscopic data (Fig. 3), results in significant transfer of the β electron from the occupied PCA $\pi_{op\text{-}sym}$ orbital into the unoccupied β d_{xz} orbital. This transfer would compensate the Fe for the donation of an α electron to O_2. However, because the d_{xz} orbital is the lowest-energy orbital in the Fe d manifold, the transfer of a β electron from the PCA to Fe and an α electron from Fe to O_2 results in an excited intermediate spin state (S = 3/2) on the Fe center (Fig. 4*C*).

In the following sections, we consider the O_2 reaction coordinate leading to the bridging peroxo complex along the S_{tot} = 3/2 surface and explore the geometric changes involved in stabilizing the intermediate spin on the Fe^{III} center. We also will discuss this reaction coordinate in the context of the mechanisms for overcoming the spin-forbidden nature of the O_2 reaction in the intradiol dioxygenases.

Reaction Coordinate to Form the Peroxy ESO_2 Complex

O_2 can interact with the Fe center and the hydroxylated carbon of catecholic substrate either sequentially or in a concerted manner in the formation of the peroxy ESO_2 complex. Previous experimental and theoretical studies showed that the ES complex of 3,4-PCD has little Fe^{II} character (20, 25, 26, 36); thus, direct interaction of O_2 at the iron center as the first step of the reaction is unlikely. To determine whether the substrate is the initial site of O_2 attack, we performed density functional theory calculations using an experimentally calibrated methodology developed in ref. 36 on hypothetical Ga^{III} catecholate and semiquinone complexes. These complexes have a similar ligand environment to the enzyme active site. Because Ga^{III} is diamagnetic with the d^{10} manifold strongly stabilized relative to the valence orbitals of the catecholic substrate, the metal d orbitals cannot participate in an interaction with O_2, which allows evaluation of whether triplet oxygen can directly attack the substrate in its two limiting electronic descriptions (catecholate and semiquinone). Geometry optimizations of these Ga^{III} complexes with O_2 showed that triplet O_2 does not interact with Ga^{III}-catecholate. While a bridging superoxy complex is formed with Ga^{III}-semiquinone, this adduct is 13 kcal/mol higher in energy than the nonbonding species, indicating that the direct attack of O_2 on PCA in the ES complex of 3,4-PCD also is unlikely. This result is consistent with previous theoretical studies (32, 37) and suggests that O_2 does not attack the iron center or the catecholate of the ES complex in a sequential manner.

Binding O_2 to the ES complex of 3,4-PCD results in a S_{tot} = 3/2 complex with Fe–O^{O2} = 2.11 Å, O–$C3^{PCA}$ = 2.61 Å and O–$C4^{PCA}$ = 2.63 Å (Fig. 5*A*). Formation of this O_2 complex is exothermic by 3.5 kcal/mol, and molecular orbital analysis shows that O_2 interacts with both Fe and PCA in this complex (Fig. 6). This orbital interaction suggests that O_2 attacks the iron and the catecholate in a concerted fashion. To form the bridging peroxo intermediate, the distal oxygen has to attack either of the hydroxylated carbons (C3 or C4). Reaction coordinates along the Fe–O^{O2} bond and either of the O–$C3^{PCA}$ and O–$C4^{PCA}$ bonds for S_{tot} = 3/2 were calculated, and the 2D energy profile along the O–$C4^{PCA}$ reaction coordinate with a double-ξ basis set (6–31G*/3–21G*) in vacuum is shown in Fig. 7. A transition state is located at Fe–O^{O2} = 1.83 Å and O–$C4^{PCA}$ = 1.92 Å, with an imaginary frequency of −300 cm^{-1} (Fig. 5*B*). The vibrational motion of this mode corresponds to the distal O atom moving toward $C4^{PCA}$ and the $O3^{PCA}$ moving away from the Fe center. After the tran-

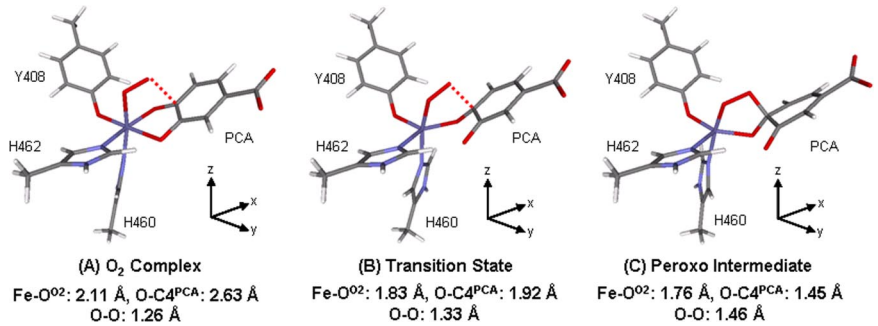

Fig. 5. Geometry optimized structures of the O_2 complex (*A*), transition state (*B*), and peroxo intermediate (*C*) obtained in the reaction coordinate calculation along Fe–O^{O2} and O–$C4^{PCA}$. Their corresponding axes are included with the structures.

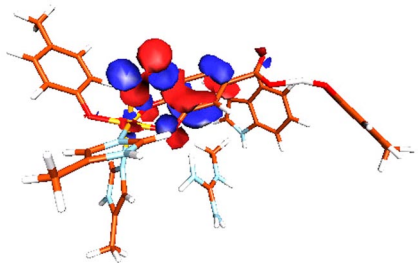

Fig. 6. Molecular orbital demonstrating the concerted interactions of Fe and PCA with O_2 in the S_{tot} = 3/2 O_2 complex.

sition state, the peroxo-bridged complex is formed. The peroxy bridged quinone substrate now binds monodentate through $O4^{PCA}$ to form a five-coordinate (5C) Fe center (Fig. 5*C*). More accurate energies of all of the optimized structures were calculated with a triple-ξ basis set (TZVP), including solvation effects (polarized continuum model with a dielectric constant ε = 4.0) and zero-point and thermal corrections and are reported in this Perspective unless otherwise specified. The transition state for the formation of the peroxo intermediate bridging to $C4^{PCA}$ (Fig. 5*B*) is 12.2 kcal/mol higher in energy than the O_2 complex (Fig. 5*A*). The overall reaction is slightly exothermic by 1.9 kcal/mol. The barrier of the peroxo formation can be attributed to the geometry change along the reaction coordinate. As the reaction proceeds from the six-coordinate (6C) O_2 complex to the transition state, the Fe–$O3^{PCA}$ bond lengthens from 2.05 Å to 2.61 Å while the Fe–O^{O2} bond shortens from 2.11 Å to 1.83 Å. This leads to a 5C site at the Fe^{III} center. However, because the bond between the distal oxygen and the substrate has not yet formed (O–$C4^{PCA}$ = 1.92 Å), this 5C structure is destabilized relative to the 6C O_2 complex. As the O–C4 distance shortens, the bond between the distal oxygen and the substrate forms and the energy of the final peroxo product is stabilized relative to the transition state. Intrinsic reaction coordinate calculations toward both reactant and product directions at the transition state result in structures that look similar to the 6C O_2 and the 5C peroxy complexes, respectively. This result confirms the presence of an accessible reaction pathway for the geometric change observed in the enzyme active site.

The energy profile along the O–$C3^{PCA}$ reaction coordinate with S_{tot} = 3/2 (data not shown) also leads to the formation a 5C bridging peroxo intermediate, but the monodentate substrate binds through $O3^{PCA}$ instead of $O4^{PCA}$. The formation of this peroxo intermediate is exothermic by 0.5 kcal/mol. Hence, in terms of the energetics for the formation of the peroxo intermediate, there is no preference in C3 versus C4 attack by the distal oxygen, but the asymmetry of the Fe–O^{PCA} bonds (Fe–$O3^{PCA}$ = 2.47 Å, Fe–$O4^{PCA}$ = 1.97 Å) observed in the crystal structure of the ES complex would facilitate the dissociation of the Fe–$O3^{PCA}$ bond in the attack of O_2 at $C4^{PCA}$, favoring this reaction. In this and the next section, we focus on the coordinate for O_2 attack at C_4^{PCA} to understand the mechanism for overcoming the spin-forbiddeness of the O_2 reaction.

As discussed in the previous section, the initial O_2 attack with S_{tot} = 5/2 is unfavorable because the O_2 molecule has an excited singlet state character. However, the total energy of the S_{tot} = 5/2 system decreases dramatically as the interaction between the singlet O_2 molecule and the ES complex is increased. Upon formation of the O_2 complex, the total energy of the S_{tot} = 5/2 system decreases from being 38.3 kcal/mol higher than the S_{tot} = 3/2 complex to only 3.6 kcal/mol. The energy profile along the O–$C4^{PCA}$ reaction coordinate of the S_{tot} = 5/2 O_2 complex (Fig. 7, red) shows that the energy barrier for the formation of the 5C peroxo intermediate is only 3.7 kcal/mol. This is significantly lower than the 12.2 kcal/mol observed in the S_{tot} = 3/2 reaction but the total energy of the final 5C peroxo species in the S_{tot} = 5/2 reaction is 4.1 kcal/mol less stable than the S_{tot} = 3/2 product. Thus, the S_{tot} = 5/2 surface intersects with the S_{tot} = 3/2 surface at two different positions (Fig. 7*B*); the first is near the beginning of the reaction coordinate (Fe–O^{O2} = 1.95 Å, O–$C4^{PCA}$ = 2.40 Å) and the second is after the S_{tot} = 3/2 transition state (Fe–O^{O2} = 1.90 Å, O–$C4^{PCA}$ = 1.80 Å). Although S_{tot} = 3/2 is the more favorable reaction path for the initial O_2 attack, intersystem crossing from S_{tot} = 3/2 to S_{tot} = 5/2 at the first intersection point of the two potential surfaces could, in principle, favor the overall energetics of the peroxy formation. However, differences in electronic as well as geometric structure between the two isoenergetic structures at the crossing point govern the feasibility of the intersystem crossing between these two spin surfaces. In the section below, we evaluate the viability of this intersystem crossing and present an alternative description of the mechanism for overcoming the spin-forbidden nature of the O_2 reaction.

Mechanism for Overcoming the Spin-Forbidden Reaction

For facile spin-crossover from the S_{tot} = 3/2 to S_{tot} = 5/2 surfaces, the two species are required to have similar geometries and energies. Moreover, the electronic structures must be able to spin-orbit couple. Spin-orbit coupling (SOC) is effectively a localized, single-center, one-electron operator and can be written as

$$L\cdot S = \frac{1}{2}[L_+S_- + L_-S_+] + L_zS_z. \quad [1]$$

The $L_+S_- + L_-S_+$ operator in Eq. **1** performs a spin-flip and this process is accompanied by a change in the orbital due to the associated L_+/L_- raising/lowering operator. Hence, the two orbitals of opposite spins involved in SOC have to be on the same center with different spatial components. SOC can also proceed through the L_zS_z operator between microstates having the same M_s for the two different S_{tot} states. In our case, this means coupling between the M_s = 3/2 microstates of the S_{tot} = 3/2 and 5/2 states. This mechanism of SOC is feasible only if the two microstates differ solely in the occupation of two orbitals

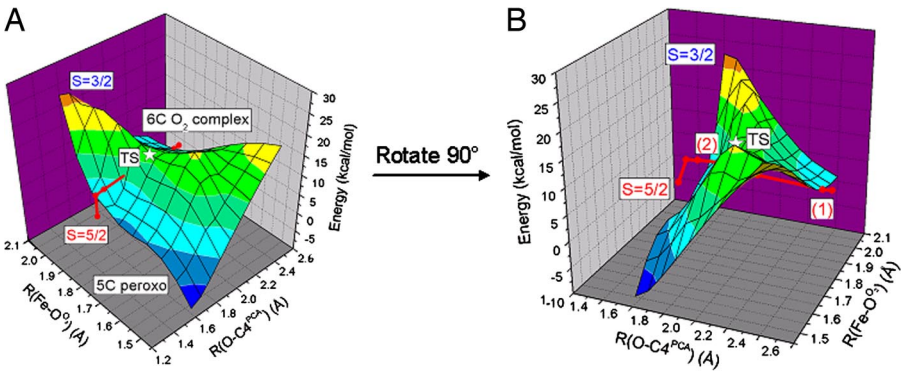

Fig. 7. O_2 reaction coordinate for 3,4-PCD. (*A*) Two-dimensional potential energy surface along R(O–$C4^{PCA}$) and R(Fe–O^{O2}) reaction coordinates for S_{tot} = 3/2 and S_{tot} = 5/2 (red). (*B*) The two crossing points (1 and 2) between S_{tot} = 3/2 and S_{tot} = 5/2. The energies are obtained with BP86 + 10% Hartree–Fock exchange and 6–31G*/3–21G* basis set in vacuum.

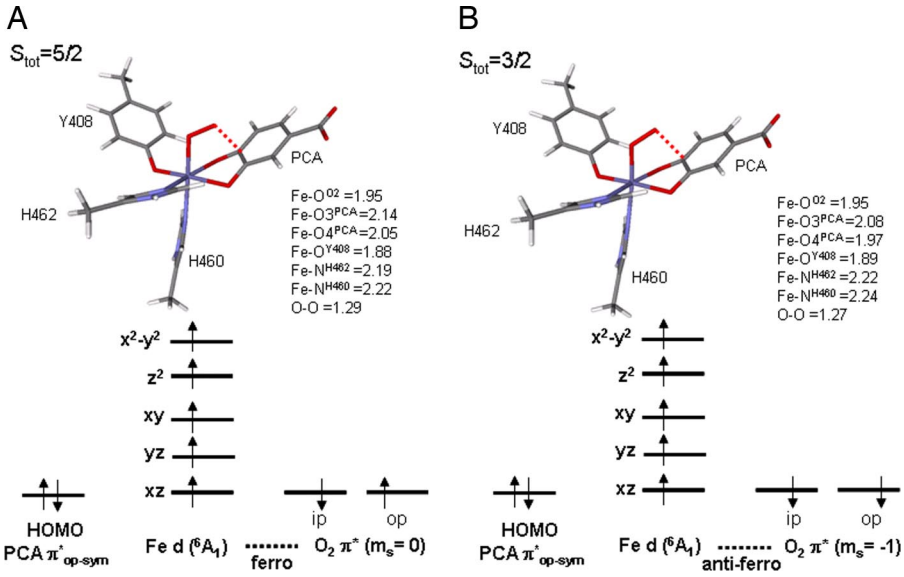

Fig. 8. Optimized geometry and electronic structures of the ESO_2 complex at the crossing point (Fe–O = 1.95 Å, O–C4 = 2.4 Å) of the S_{tot} = 5/2 and S_{tot} = 3/2 O-C4^{PCA} reaction coordinates: S_{tot} = 5/2 (*A*) and S_{tot} = 3/2 (*B*).

with the same spin and these two orbitals can couple through L_z.

The two isoenergetic structures for S_{tot} = 5/2 and 3/2 at the second crossing point along the O–C4^{PCA} reaction coordinate have very different geometries; hence, intersystem crossing is not feasible. However, as shown in Fig. 8, the two isoenergetic structures for S_{tot} = 5/2 and 3/2 at the first crossing point have similar geometries. It only takes 3.1 kcal/mol to excite the S_{tot} = 3/2 electronic configuration in its optimized structure into a S_{tot} = 5/2 state. Hence, it is energetically feasible for intersystem crossing. Orbital analysis on the S_{tot} = 5/2 structure shows significant overlap between the doubly occupied PCA $\pi_{op\text{-}sym}$ orbital and the O_2 molecule (m_s = 0) in which the two π^* orbitals are occupied by two electrons of opposite spin (β in π^*_{ip} and α in π^*_{op}, with the in-plane (ip) and out-of-plane (op) orbitals defined by the Fe–O–O plane). For the S_{tot} = 3/2 structure, a covalent interaction between the PCA $\pi_{op\text{-}sym}$ and O_2 π^*_{ip} in the α manifold is observed while the O_2 π^*_{op} orbital remains singly occupied by a β electron. For both spin states, the iron center remains high-spin ferric with strong bonding interactions with PCA. Hence, the major difference in the electronic structure between the two spin states at the crossing point lies in the spin of the electron residing in the singly occupied π^*_{op}, with α for S_{tot} = 5/2 and β for S_{tot} = 3/2 (Fig. 8). Although both of these spin orbitals are localized on O_2, they have the same spatial component in their wave functions (π^*_{op}). Hence, the S_{tot} = 3/2 surface cannot effectively intersystem cross to the S_{tot} = 5/2 surface through the SOC mechanism at this point of the potential energy surface as the orbital angular momentum operators associated with SOC in Eq. **1** require a change in orbital occupation. Thus, the O_2 reaction with the ES complex should remain on the S_{tot} = 3/2 surface from the initial attack at the Fe center through the formation of the bridging peroxo complex.

To understand how the spin forbiddeness of the O_2 reaction is overcome on the S_{tot} = 3/2 surface, electronic structures at three points along the O–C4 reaction coordinate are considered: (*i*) the O_2 complex, (*ii*) the transition state, and (*iii*) the final bridged peroxo intermediate. The amount of charge transfer among the five Fe d orbitals, the PCA $\pi_{op\text{-}sym}$ orbital and the two O_2 π^* orbitals were quantified by calculating the total percentage of orbital occupancy and assigning the major bonding partner(s) for each of the orbitals in both α and β spins. For example, in the ES complex, the β PCA $\pi_{op\text{-}sym}$ orbital is 61% occupied (summed over all occupied molecular orbitals), and the remaining 39% is contributed in the three unoccupied Fe β d_π orbitals, with 18% on d_{xz}. Thus the Fe β d_{xz} orbital is the major bonding partner of the β PCA $\pi_{op\text{-}sym}$, and a total of 0.39 e^- has been transferred from the β PCA $\pi_{op\text{-}sym}$ to the Fe β d_π manifold. The electron transfers among orbitals for the three different points along the reaction coordinates are summarized in Fig. 9.

O_2 Complex [Figs. 5*A* (Geometry) and 9*A* (Electronic Structure)]. The Fe–O_2 bond is defined as the *z* axis with the two Fe–O^{PCA} bonds defining the *x* and *y* axes. The energy ordering of the Fe d orbitals is as follows: $d_{xz} < d_{yz} < d_{xy} < d_{z^2} < d_{x^2-y^2}$. Because the dihedral angle between the Fe–O–O and O–O–C4 planes is 14.5°, our frontier molecular orbital analysis in ref. 36 predicted that O_2 π^*_{ip} will directly overlap with the PCA $\pi_{op\text{-}sym}$ orbital. Consistent with this model, 0.42 e^- is donated directly from the α PCA $\pi_{op\text{-}sym}$ to the α O_2 π^*_{ip}, whereas 0.37 e^- is donated

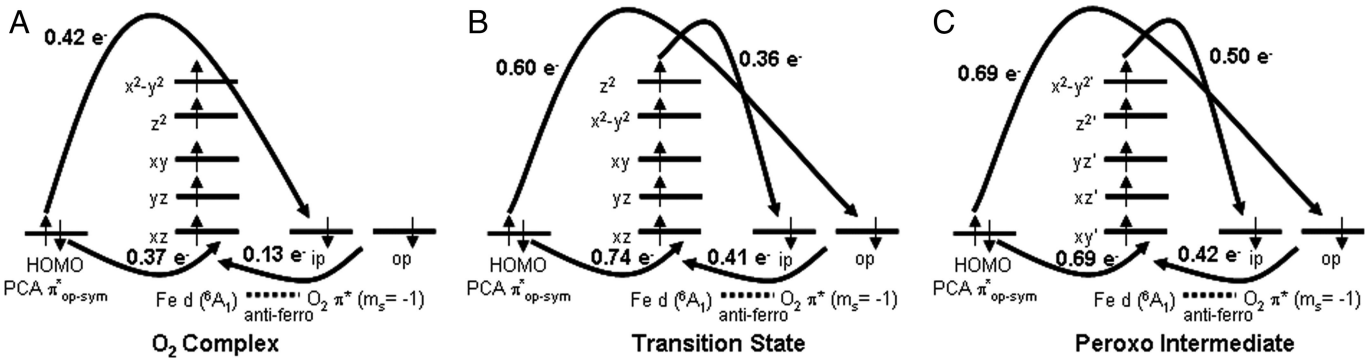

Fig. 9. Schematics of electron transfer at three different points along the O–C4^{PCA} reaction coordinates: O_2 complex (*A*), transition state (*B*), and peroxo intermediate (*C*).

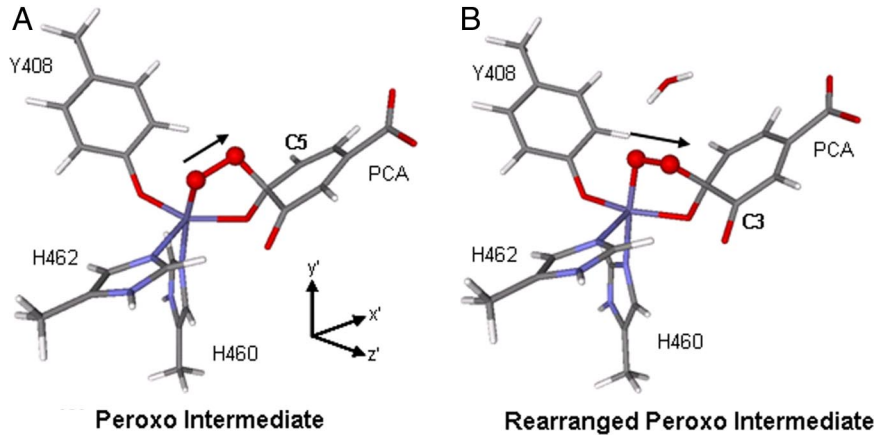

Fig. 10. Geometries of peroxo intermediates: optimized peroxo intermediate (*A*), rearranged peroxo intermediate optimized with hydrogen bonding from water (*B*). The black arrow indicates the O–O bond vector.

through covalent bonding between β PCA $\pi_{op\text{-}sym}$ and Fe β d_{xz}, as observed in our spectroscopic studies of the ES complex (Fig. 3) (36). The small charge transfer from the occupied β O_2 π^* orbitals to the unoccupied Fe β d orbitals reflects the covalent interactions between O_2 and Fe. The net result is that PCA starts to gain more semiquinone character as a total of 0.79 e^- is lost from the PCA $\pi_{op\text{-}sym}$ and the electronic description of the Fe–O_2 unit is between the two limiting cases, Fe^{II}–O_2^- and Fe^{III}–O_2.

Transition State [Figs. 5*B* (Geometry) and 9*B* (Electronic Structure)]. Due to the lengthening of the Fe–$O3^{PCA}$ bond and the contraction of the Fe–$O^{peroxide}$ bond, the active site now adopts an intermediate structure between square pyramidal and trigonal bipyramidal. The energy ordering of the Fe d orbitals in the same molecular coordinate system as defined in the O_2 complex is as follows: $d_{xz} < d_{yz} < d_{xy} < d_{x^2-y^2} < d_{z^2}$. The dissociation of the Fe–$O3^{PCA}$ bond allows the remaining three equatorial ligands (Tyr-408, His-462, and $O4^{PCA}$) to reorganize in the plane and leads to the stabilization of the d_{xz} orbital. On the other hand, the destabilization of the d_{z^2} orbital is attributed to the strong Fe–$O^{peroxide}$ bond. Due to the large geometric rearrangement to produce the 5C Fe center, the Fe–O–O–$C4^{PCA}$ dihedral angle increases in magnitude from 14.5° to −35.0°, which allows direct overlap between the α PCA $\pi_{op\text{-}sym}$ and O_2 π^*_{op} orbitals. The charge transfer pattern in the O_2 complex also is observed in the transition state: 0.60 e^- from the α PCA $\pi_{op\text{-}sym}$ to the α O_2 $^*_{op}$, 0.74 e^- from β PCA $\pi_{op\text{-}sym}$ to Fe β d_{xz} and 0.41 e^- from the β O_2 π^* to the Fe β d orbitals. There also is charge transfer of 0.36 e^- from the Fe α d_{z^2} orbital to the α O_2 π^*_{ip} orbital at the transition state. These results demonstrate that the two α electrons involved in reducing O_2 to O_2^{2-} come from two different sources, one from the catecholic substrate and the other from the Fe center. Due to the ligand rearrangement, the α electron transfer from the Fe proceed through the good overlap between the highest energy d orbital (d_{z^2}) and the O_2 π^*_{ip} orbital. However, this is compensated by the β donation from the PCA to the Fe d_π orbitals and results in an S = 3/2 intermediate spin electronic configuration at the Fe^{III} center. The S = 3/2 is now in its ground state as the distorted trigonal bipyramidal structure around the Fe center stabilizes this electronic configuration. Considering the total e^- gain and loss in the O_2 π^* and PCA $\pi_{op\text{-}sym}$ orbitals, respectively, the O_2 has been reduced to a superoxide, while the PCA is at the semiquinone level at the transition state.

Final Peroxo Intermediate [Figs. 5*C* (Geometry) and 9*C* (Electronic Structure)]. The active site becomes more trigonal bipyramidal with the axial direction defined by the short Fe–$O^{peroxide}$ bond. The charge transfer pattern of this peroxo intermediate is the same as in the transition state, except that the two-electron redox process between the PCA and the O_2 molecule is now complete. The same amount of α and β spins of the PCA $\pi_{op\text{-}sym}$ orbital are transferred to the α O_2 π^*_{ip} and Fe β d_{xz} orbitals, respectively. The α electron transfer from the Fe d_{z^2} orbital to the O_2 π^*_{ip} has increased to 0.50 e^-. These results show that three different electron transfer processes (one β and two α) are involved with no spin flip in the formally spin-forbidden, two-electron redox process between the singlet catecholate and the triplet O_2.

While the α electron of the singlet substrate can have direct overlap with the triplet O_2 molecule, its β counterpart cannot be transferred directly to the O_2 molecule without a spin-flip process. The Fe^{III} center in the intradiol dioxygenases thus plays a critical role in overcoming the spin-forbidden nature of the O_2 reaction. The strong covalent interaction between the substrate and the iron center, as reflected in the low-energy spectroscopic feature of the ES complex (Fig. 3), allows the transfer of this β electron from the substrate to the metal. With the metal acting as a buffer, an electron of the appropriate spin (α) can be transferred to the O_2 molecule to complete the two-electron redox process. However, this would leave the iron center in an excited intermediate spin state (S = 3/2). The ligand field geometry change at the Fe center along the reaction coordinate is key in stabilizing this intermediate spin configuration. As the catecholic substrate is oxidized, the iron loses the Fe–$O3^{PCA}$ bond in the equatorial plane and the bonding interaction between the Fe and O_2 is strengthened in the axial direction, producing a trigonal bipyramidal ligand field with a strong axial bond, which destabilizes the d_{z^2} orbital and stabilizes the intermediate S_{tot} = 3/2 spin state on the ferric center.

The Reaction Coordinate

As developed in the previous section, the O_2 reaction with the ES complex remains on the S_{tot} = 3/2 surface from the initial attack at the Fe center all of the way through the formation of the bridging peroxo complex. However, experimental data show that the ferric center is high-spin, S = 5/2, at the beginning and end of the catalytic cycle; hence, the 5C S_{tot} = 3/2 peroxo intermediate must return to the S_{tot} = 5/2 reaction surface. Inspection of the 6C O_2 complex and the 5C peroxo species shows that, although the three endogenous ligands show very little change in their positions, the $O^{Tyr\text{-}408}$–Fe–$O4^{PCA}$ angle has increased from 100.7° to 135.7° as the peroxo is formed and the Fe–$O3^{PCA}$ bond is lost. This geometric change is due to the swinging of the Fe–$O4^{PCA}$ bond away from the trans position of His-462. Such geometric arrangement is very similar to those observed in the crystal structures of enzyme–inhibitor complexes (38). In these inhibitor complexes, Tyr-447 becomes the ligand trans to His-462. Opening the $O^{Tyr\text{-}408}$–Fe–$O4^{PCA}$ angle in the peroxy species would allow coordination of a sixth ligand, either Tyr-447 or a solvent water molecule. Kinetics studies of the O_2 reaction of both the wild-type enzyme and the Y447H mutant show similar spectroscopic features for the two oxygen intermediates,

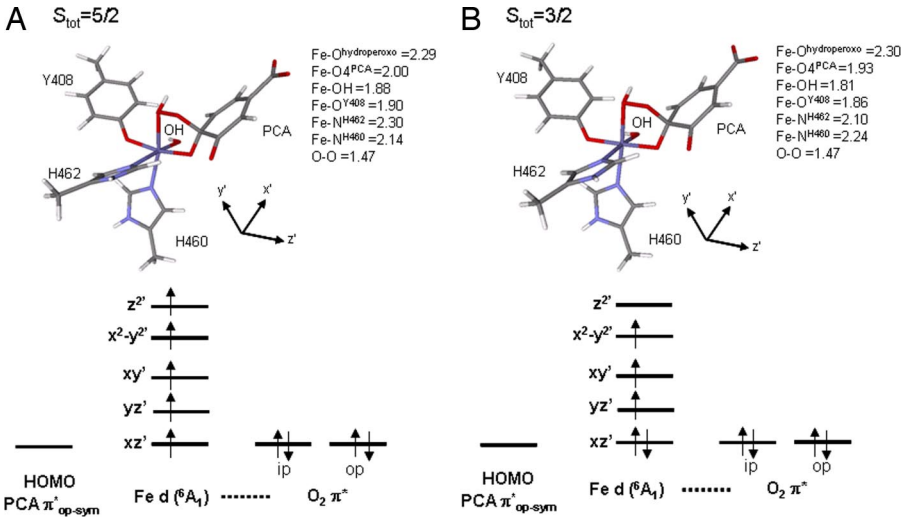

Fig. 11. Optimized geometry and electronic structures of the 6C hydroperoxo complex for both S_{tot} = 5/2 (*A*) and S_{tot} = 3/2 (*B*).

ESO_2 and ESO_2^*, with the latter being the enzyme–product complex (39). The absence of additional spectral features in the oxygen intermediates of the wild-type enzyme relative to the Y447H mutant strongly suggests the sixth ligand that binds to the 5C peroxo species is a water molecule. In the previous section, we emphasized how the intermediate spin state on the Fe^{III} center is stabilized by a change in coordination number from 6 to 5 and the associated ligand field as the peroxo complex is formed. Thus, we expect the change in ligand field as the sixth ligand binds to the 5C peroxo complex would allow the S_{tot} = 3/2 peroxo complex to return to S_{tot} = 5/2 and complete the catalytic reaction.

Attempts to bind a water to the open site of the S_{tot} = 3/2 peroxo species lead to a very long Fe–O^{H2O} distance of 3.61 Å, where the water is held weakly to Fe^{III} active site through hydrogen bonding with the catecholic substrate. However, if the water molecule is added to the active site such that it is allowed to hydrogen-bond to the peroxo bridge, an interesting geometric change is observed. The O–O bond vector changes from pointing toward $C5^{PCA}$, as in the 5C peroxo complex, to pointing toward $C3^{PCA}$ (Fig. 10). Such a rearrangement for the S_{tot} = 5/2 species has been proposed by Siegbahn *et al.* (37) to be important in producing intradiol-cleaved product. Upon formation of this rearranged 5C peroxo species, proton donation from H_2O to the peroxo unit results in OH^- binding to the open coordination site. Geometry optimization of the 6C bridging hydroperoxy complex at both S_{tot} = 3/2 and S_{tot} = 5/2 shows that the latter species is now more stable by 2.8 kcal/mol. The geometric and electronic structures of these two bridging hydroperoxy adducts are shown in Fig. 11. Both of the structures are octahedral at the Fe^{III} center, with the Fe–$O^{hydroperoxo}$ bond lengthened to ≈2.3 Å. The 5C strong axial trigonal bipyramidal stabilization for the intermediate spin we observe for the peroxo species is no longer present. Comparing the electronic structures of the 6C hydroperoxo species in the two different spin states and using the coordinate system in Fig. 11, we can see that SOC between $d_{xz'}$ and $d_{z^2'}$ in the S_{tot} = 3/2 adduct through L_y would allow for intersystem crossing and the Fe^{III} center can now return to the S_{tot} = 5/2 state. We have considered the energetics for O–O bond cleavage following the formation of this S_{tot} = 5/2 hydroperoxy adduct that lead to the formation of an anhydride intermediate. The results are similar to those reported by Siegbahn *et al.* (37) and, thus, will not be further discussed in this Perspective.

In summary, coordination of the sixth ligand to the 5C S_{tot} = 3/2 peroxo adduct results in a ligand field change that allows the Fe^{III} center to return to the S_{tot} = 5/2 reaction surface and complete the catalytic cycle.

Concluding Comments

We have developed a mechanism in which the high-spin ferric active site of the intradiol dioxygenases can use its coordination environment to tune the ligand field around the metal center to allow a change in spin state from S = 5/2 to S = 3/2 along the reaction coordinate, which involves the transfer of three electrons without a change in their spins. The intermediate S = 3/2 spin state is accessible to the Fe^{III} center upon O_2 binding and dissociation of an Fe–$O^{catecholate}$ bond. This provides a mechanism for overcoming the spin-forbidden nature of the reaction between the triplet O_2 and singlet organic substrates. This 5C S_{tot} = 3/2 peroxo intermediate must return to the S_{tot} = 5/2 surface to complete the reaction and this can be accomplished by coordination of H_2O to the open position in the Fe^{III} center. H_2O coordination also provides a proton for the O–O bond cleavage and the insertion of an O atom for the intradiol dioxygenation.

This research was supported by National Institutes of Health Grants GM40392 (to E.I.S.) and GM24689 (to J.D.L.). M.Y.M.P. thanks the Natural Sciences and Engineering Research Council of Canada for a postgraduate scholarship.

1. Feig AL, Lippard SJ (1994) *Chem Rev* 94:759–805.
2. Hegg EL, Que L, Jr (1997) *Eur J Biochem* 250:625–629.
3. Lipscomb JD, Orville AM (1992) *Metal Ions Biol Syst* 28:243–298.
4. Que L, Jr, Ho RYN (1996) *Chem Rev* 96:2607–2624.
5. Solomon EI, Brunold TC, Davis MI, Kemsley JN, Lee SK, Lehnert N, Neese F, Skulan AJ, Yang YS, Zhou J (2000) *Chem Rev* 100:235–349.
6. Gardner HW (1991) *Biochim Biophys Acta* 1084:221–239.
7. Siedow JN (1991) *Annu Rev Plant Physiol Plant Mol Biol* 42:145–188.
8. Yamamoto S (1992) *Biochim Biophys Acta* 1128:117–131.
9. Ford-Hutchinson AW, Gresser M, Young RN (1994) *Annu Rev Biochem* 63:383–417.
10. Kühn H, Borngräber S (1999) in *Lipoxygenases and Their Metabolites*, eds Nigam S, Pace-Asciak CR (Plenum, New York), pp 5–28.
11. Boyington JC, Gaffney BJ, Amzel LM (1993) *Science* 260:1482–1486.
12. Minor W, Steczko J, Stec B, Otwinowski Z, Bolin JT, Walter R, Axelrod B (1996) *Biochemistry* 35:10687–10701.
13. Tomchick DR, Phan P, Cymborowski M, Minor W, Holman TR (2001) *Biochemistry* 40:7509–7517.
14. Nelson MJ, Seitz SP (1994) *Curr Opin Struct Biol* 4:878–884.
15. Solomon EI, Zhou J, Neese F, Pavel EG (1997) *Chem Biol* 4:795–808.
16. Holman TR, Zhou J, Solomon EI (1998) *J Am Chem Soc* 120:12564–12572.
17. Gardner KA, Mayer JM (1995) *Science* 269:1849–1851.
18. Bugg TDH, Winfield CJ (1998) *Nat Prod Rep* 513–530.
19. Bugg TDH, Lin G (2001) *Chem Commun* 941–952.
20. True AE, Orville AM, Pearce LL, Lipscomb JD, Que L, Jr (1990) *Biochemistry* 29:10847–10854.
21. Ohlendorf DH, Orville AM, Lipscomb JD (1994) *J Mol Biol* 244:586–608.

22. Davis MI, Orville AM, Neese F, Zaleski JM, Lipscomb JD, Solomon EI (2002) *J Am Chem Soc* 124:602–614.
23. Orville AM, Lipscomb JD, Ohlendorf DH (1997) *Biochemistry* 36:10052–10066.
24. Horsman GP, Jirasek A, Vaillancourt FH, Barbosa CJ, Jarzecki AA, Xu CL, Mekmouche Y, Spiro TG, Lipscomb JD, Blades MW, *et al*. (2005) *J Am Chem Soc* 127:16882–16891.
25. Que L, Jr, Lipscomb JD, Zimmerman R, Münck E, Orme-Johnson NR, Orme-Johnson WH (1976) *Biochim Biophys Acta* 452:320–334.
26. Whittaker JW, Lipscomb JD, Kent TA, Münck E (1984) *J Biol Chem* 259:4466–4475.
27. Que L, Jr, Lipscomb JD, Munck E, Wood JM (1977) *Biochim Biophys Acta* 485:60–74.
28. Cox DD, Que L, Jr (1988) *J Am Chem Soc* 110:8085–8092.
29. Jang HG, Cox DD, Que L, Jr (1991) *J Am Chem Soc* 113:9200–9204.
30. Lipscomb JD, Orville AM, Frazee RW, Dolbeare KB, Elango N, Ohlendorf DH (1998) in *Spectroscopic Methods in Bioinorganic Chemistry*, eds Solomon EI, Hodgson KO (Am Chem Soc, Washington, DC), pp 387–402.
31. Funabiki T, Konishi T, Kobayashi S, Mizoguchi A, Takano M, Yoshida S (1987) *Chem Lett* 719–722.
32. Funabiki T, Yamazaki T (1999) *J Mol Catal A* 150:37–47.
33. Hitomi Y, Yoshida M, Higuchi M, Minami H, Tanaka T, Funabiki T (2005) *J Inorg Biochem* 99:755–763.
34. Kim M, Okajima T, Kishishita S, Yoshimura M, Kawamori A, Tanizawa K, Yamaguchi H (2002) *Nat Struct Biol* 9:591–596.
35. Dove JE, Schwartz B, Williams NK, Klinman JP (2000) *Biochemistry* 39:3690–3698.
36. Pau MYM, Davis MI, Orville AM, Lipscomb JD, Solomon EI (2007) *J Am Chem Soc* 129:1944–1958.
37. Borowski T, Siegbahn PEM (2006) *J Am Chem Soc* 128:12941–12953.
38. Orville AM, Elango N, Lipscomb JD, Ohlendorf DH (1997) *Biochemistry* 36:10039–10051.
39. Frazee RW, Orville AM, Dolbeare KB, Yu H, Ohlendorf DH, Lipscomb JD (1998) *Biochemistry* 37:2131–2144.